Peroxidasin-mediated bromine enrichment of basement membranes

Cuiwen He[a,1], Wenxin Song[a,1], Thomas A. Weston[a], Caitlyn Tran[a], Ira Kurtz[a], Jonathan E. Zuckerman[b], Paul Guagliardo[c], Jeffrey H. Miner[d], Sergey V. Ivanov[e,f], Jeremy Bougoure[c], Billy G. Hudson[e,f,g,h], Selene Colon[e,f,h,i], Paul A. Voziyan[e,f], Gautam Bhave[e,f,i,j], Loren G. Fong[a], Stephen G. Young[a,k,2,3], and Haibo Jiang[l,m,2,3]

[a]Department of Medicine, University of California, Los Angeles, CA 90095; [b]Department of Pathology and Laboratory Medicine, University of California, Los Angeles, CA 90095; [c]Centre for Microscopy, Characterisation and Analysis, University of Western Australia, 6009 Perth, Australia; [d]Division of Nephrology, Washington University School of Medicine, St. Louis, MO 63110; [e]Vanderbilt Center for Matrix Biology, Vanderbilt University Medical Center, Nashville, TN 37212; [f]Division of Nephrology, Department of Medicine, Vanderbilt University Medical Center, Nashville, TN 37232; [g]Vanderbilt Ingram Cancer Center, Vanderbilt University Medical Center, Nashville, TN 37232; [h]Vanderbilt Institute of Chemical Biology, Vanderbilt University, Nashville, TN 37232; [i]Department of Cell and Developmental Biology, Vanderbilt University, Nashville, TN 37212; [j]Center for Kidney Disease, Vanderbilt University Medical Center, Nashville, TN 37232; [k]Department of Human Genetics, University of California, Los Angeles, CA 90095; [l]School of Molecular Sciences, University of Western Australia, 6009 Perth, Australia; and [m]Department of Chemistry, The University of Hong Kong, Hong Kong, China

Contributed by Stephen G. Young, May 25, 2020 (sent for review April 22, 2020; reviewed by Douglas Gould and Martin R. Pollak)

Bromine and peroxidasin (an extracellular peroxidase) are essential for generating sulfilimine cross-links between a methionine and a hydroxylysine within collagen IV, a basement membrane protein. The sulfilimine cross-links increase the structural integrity of basement membranes. The formation of sulfilimine cross-links depends on the ability of peroxidasin to use bromide and hydrogen peroxide substrates to produce hypobromous acid (HOBr). Once a sulfilimine cross-link is created, bromide is released into the extracellular space and becomes available for reutilization. Whether the HOBr generated by peroxidasin is used very selectively for creating sulfilimine cross-links or whether it also causes oxidative damage to bystander molecules (e.g., generating bromotyrosine residues in basement membrane proteins) is unclear. To examine this issue, we used nanoscale secondary ion mass spectrometry (NanoSIMS) imaging to define the distribution of bromine in mammalian tissues. We observed striking enrichment of bromine (^{79}Br, ^{81}Br) in basement membranes of normal human and mouse kidneys. In peroxidasin knockout mice, bromine enrichment of basement membranes of kidneys was reduced by ∼85%. Proteomic studies revealed bromination of tyrosine-1485 in the NC1 domain of α2 collagen IV from kidneys of wild-type mice; the same tyrosine was brominated in collagen IV from human kidney. Bromination of tyrosine-1485 was reduced by >90% in kidneys of peroxidasin knockout mice. Thus, in addition to promoting sulfilimine cross-links in collagen IV, peroxidasin can also brominate a bystander tyrosine. Also, the fact that bromine enrichment is largely confined to basement membranes implies that peroxidasin activity is largely restricted to basement membranes in mammalian tissues.

collagen IV | sulfilimine cross-links | NanoSIMS imaging | bromine | bromotyrosine

Six years ago, bromine was shown to be an essential element, required for the formation of sulfilimine cross-links in collagen IV (1). Collagen IV is a trimeric molecule generated from six different collagen IV isomers (α1–α6) and is a crucial component for basement membranes underlying epithelial cells, endothelial cells, and muscle cells (2). There are three types of collagen IV trimers: $\alpha1_2$–α2, α3–α4–α5, and $\alpha5_2$–α6. Sulfilimine cross-links link two collagen IV trimers, forming a hexamer structure. The sulfilimine cross-linking reaction is mediated by peroxidasin, an extracellular matrix (ECM) peroxidase that uses two substrates, hydrogen peroxide (H_2O_2) and bromide, to generate hypobromous acid (HOBr) (3). It has been proposed that HOBr forms a bromosulfonium intermediate in the side chain of methionine-1570 (numbering throughout this paper refers to COL4A2) located within the carboxyl-terminal noncollagenous domain (NC1 domain) of collagen IV. The bromosulfonium intermediate then promotes the formation of a sulfilimine cross-link between the methionine and a spatially adjacent hydroxylysine residue (lysine-1689) in a partner collagen IV trimer (1, 4). While bromide is required for the formation of the sulfilimine cross-links, bromide is simply an intermediate in the cross-linking reaction. H_2O_2 is consumed during the cross-linking reaction, but, following cross-linking, the bromide is released into the extracellular space (1).

The peroxidasin- and bromide-catalyzed sulfilimine cross-links buttress the structural integrity of the basement membrane (5) and are crucial in all metazoans, including in *Drosophila melanogaster*, *Caenorhabditis elegans*, and mammals (2, 4, 6). In *Drosophila*, an absence of sulfilimine cross-links, due either to peroxidasin deficiency or a deficiency in bromine, causes disorganization of basement membranes of muscle cells, leading to gut rupture and larval death (1, 7). In humans and mice, a deficiency of peroxidasin causes severe developmental abnormalities in the anterior

Significance

Bromine is an essential trace element, required for the formation of sulfilimine cross-links in collagen IV, a basement membrane protein. Sulfilimine cross-link formation depends on the production of hypobromous acid by peroxidasin. Once the cross-links are formed, bromide is released, but we suspected that hypobromous acid might brominate bystander molecules in the basement membrane. NanoSIMS imaging of mouse kidneys revealed peroxidasin-dependent bromine enrichment in the basement membrane, and proteomics studies uncovered peroxidasin-dependent bromination of a specific tyrosine in collagen IV. Our studies show that bromine, an essential element, is largely restricted to basement membranes in mammalian tissues. Our studies also show that peroxidasin brominates bystander tyrosines in addition to promoting the formation of collagen IV sulfilimine cross-links.

Author contributions: C.H., W.S., J.E.Z., L.G.F., S.G.Y., and H.J. designed research; C.H., W.S., T.A.W., C.T., I.K., J.E.Z., P.G., J.H.M., S.V.I., J.B., B.G.H., S.C., P.A.V., G.B., L.G.F., and H.J. performed research; J.H.M., S.V.I., P.A.V., and G.B. contributed new reagents/analytic tools; C.H., W.S., J.E.Z., L.G.F., S.G.Y., and H.J. analyzed data; and C.H., G.B., L.G.F., S.G.Y., and H.J. wrote the paper.

Reviewers: D.G., University of California San Francisco Medical Center; and M.R.P., Beth Israel Deaconess Medical Center.

The authors declare no competing interest.

[1]C.H. and W.S. contributed equally to this work.

[2]S.G.Y. and H.J. contributed equally to this work.

[3]To whom correspondence may be addressed. Email: sgyoung@mednet.ucla.edu or haibo.jiang@uwa.edu.au.

This article contains supporting information online at https://www.pnas.org/lookup/suppl/doi:10.1073/pnas.2007749117/-/DCSupplemental.

First published June 22, 2020.

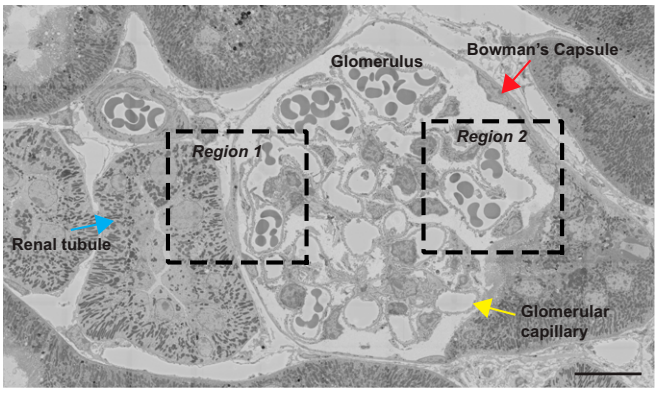

Fig. 1. Tiled BSE image of a glomerulus and surrounding renal tubules from a kidney of a wild-type mouse. Boxed regions were imaged by NanoSIMS (see Figs. 2 and 3). Red arrow, Bowman's capsule; blue arrow, renal tubule; yellow arrow, glomerular capillary. (Scale bar: 15 μm.)

chamber of the eye by disrupting the integrity of basement membranes lining lens epithelial cells (8–10).

The production of hypohalous acids by peroxidases is not unique to peroxidasin. Myeloperoxidase in polymorphonuclear leukocytes produces hypochlorous acid, which is important for destroying microorganisms within leukocyte phagolysosomes (11, 12). Eosinophil peroxidase produces HOBr (13), which assists in controlling parasitic infections (14–16). Hypohalous acids are highly reactive and known to oxidize amino acids, carbohydrates, and nucleic acids in microorganisms, explaining their utility in fighting infections, but they also react with bystander molecules of the host (7, 17). For example, the release of eosinophil peroxidase into the lung parenchyma results in HOBr, which in turn forms bromotyrosine residues (18, 19). Similarly, the myeloperoxidase in atherosclerotic plaques results in the formation of chlorotyrosine residues in bystander proteins (20, 21).

The fact that myeloperoxidase and eosinophil peroxidase can cause oxidative damage to bystander host proteins naturally raises questions about peroxidasin biology. The first is whether the HOBr produced by peroxidasin is entirely selective for promoting sulfilimine cross-links in collagen IV or whether it also covalently modifies bystander molecules within the ECM (e.g., forms bromotyrosines in basement membrane proteins). Several groups have raised the possibility that peroxidasin activity could damage bystander proteins (7, 22, 23), but there has been little experimental evidence to support this idea. Second, if peroxidasin were to covalently modify bystander proteins, would those modifications be confined to the basement membrane, or would they be more widespread within the underlying stromal/interstitial ECM between cells? Ig domains within peroxidasin are thought to facilitate indirect interactions between peroxidasin and collagen IV within the basement membrane (6). However, at this point, it is unclear whether peroxidasin activity is confined to the basement membrane or is ubiquitous within the ECM. Third, if bromination of ECM proteins occurs in mammalian tissues, would the extent of bromination be reduced by a deficiency of peroxidasin?

In the current study, our goal was to address these issues, taking advantage of a combination of mass spectrometry-based imaging (nanoscale secondary ion mass spectrometry [NanoSIMS] imaging) of mammalian tissues and mass spectrometry-based proteomic studies of basement membrane proteins. We focused our efforts on the kidney because basement membrane composition, structure, and function are highly relevant to chronic kidney disease. Mutations in three collagen IV chain genes (*COL4A3*, *COL4A4*, and *COL4A5*) cause Alport syndrome, a glomerulopathy associated with deafness (24–26). These mutations interfere with the formation of the α3–α4–α5 collagen IV trimer, which is generated by podocytes and is critical for the function of the glomerulus. Heterozygous mutations in *COL4A3* and *COL4A4* cause a related disease, thin basement membrane nephropathy (TBMN) (27). Autoantibodies against the glomerular basement membrane (GBM) collagen IV cause Goodpasture's disease (anti-GBM disease) (28). In patients with diabetic kidney disease, GBMs are thickened and dysfunctional (29).

Results

Distribution of Bromine in Mouse Tissues. Bromine is an essential element in metazoans (1), but its tissue distribution has never been defined. We examined 500-nm-thick sections of resin-embedded mouse kidney by both backscattered electron (BSE) imaging (providing high-resolution morphology of cells and tissues) and NanoSIMS analyses (generating high-resolution images based on isotopic content). Fig. 1 shows a BSE image of a glomerulus and adjacent renal tubules from a wild-type mouse. Higher magnification electron micrographs of two boxed regions (region 1 and region 2) are shown in the *Upper* panels of Figs. 2 and 3, respectively, along with ^{32}S, ^{31}P, and ^{79}Br NanoSIMS images. The ^{32}S and ^{31}P images are useful for cellular and tissue morphology, and the ^{31}P images are useful for identifying cell nuclei. NanoSIMS images of region 1 (Fig. 2, *Upper*) revealed striking ^{79}Br enrichment along the edge of a renal tubular epithelial cell, along the edge of a parietal cell in Bowman's capsule, and along a glomerular capillary. NanoSIMS images of region 2 (Fig. 3, *Upper*) revealed marked ^{79}Br enrichment along a glomerular capillary and along a parietal cell in Bowman's capsule.

Higher magnification electron micrographs of the boxed regions in the *Upper* panels of Figs. 2 and 3 (area a and area b) are shown in the *Lower* panels, along with composite ^{31}P, ^{32}S, and ^{79}Br NanoSIMS images. The higher magnification images show that ^{79}Br is confined to basement membranes, including renal tubule basement membranes (TBMs), Bowman's capsule basement membranes (BCBMs), and the GBM between podocytes and endothelial cells of glomerular capillaries.

Additional correlative BSE and NanoSIMS images of mouse glomeruli are shown in *SI Appendix*, Figs. S1 and S2, again revealing bromine enrichment in the TBMs, BCBMs, and GBMs. NanoSIMS images for ^{79}Br (50.7% natural abundance) and ^{81}Br (49.3% natural

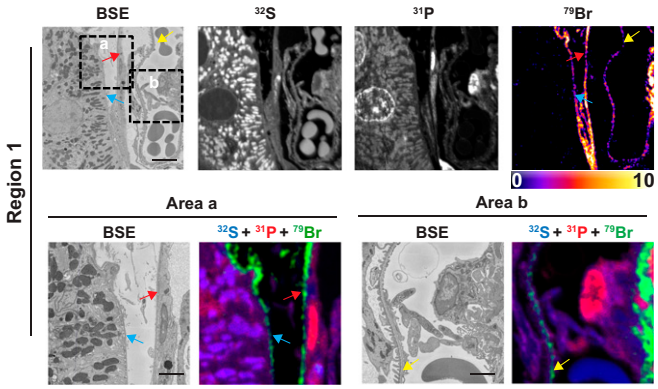

Fig. 2. Bromine is enriched in basement membranes of mouse kidney, as judged by BSE imaging and NanoSIMS analyses. Region 1 of a renal glomerulus (see Fig. 1) was mapped by BSE imaging and NanoSIMS. ^{31}P and ^{32}S images were useful for defining tissue morphology; the ^{79}Br image depicts bromine distribution. (*Lower*) Close-up images of boxed regions (area a and area b) in the *Upper*. BSE images and composite ^{31}P (red), ^{32}S (blue), and ^{79}Br (green) NanoSIMS images of area a and area b reveal bromine enrichment in the GBM (yellow arrows), the renal tubule basement membrane (blue arrows), and the basement membrane of Bowman's capsule (red arrows). (Scale bars: *Upper*, 5 μm; *Lower*, 2 μm.)

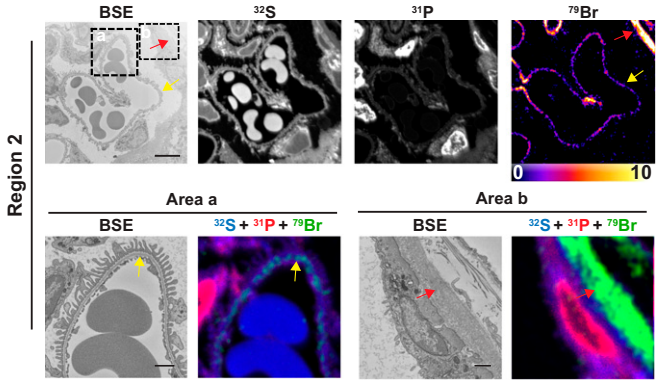

Fig. 3. Bromine is enriched in basement membranes of mouse kidney, as judged by BSE imaging and NanoSIMS analyses. Region 2 of a renal glomerulus (see Fig. 1) was mapped by BSE imaging and NanoSIMS. ^{31}P and ^{32}S images were useful for defining tissue morphology; the ^{79}Br image depicts bromine distribution within the kidney. (*Lower*) Within each region, close-up images of boxed regions (area a, area b) in the *Upper*. BSE images and composite ^{31}P (red), ^{32}S (blue), and ^{79}Br (green) NanoSIMS images of area a and area b reveal bromine enrichment in the GBM (yellow arrows) and the basement membrane of Bowman's capsule (red arrows). (Scale bars: *Upper*, 5 μm; *Lower*, 1 μm.)

abundance) were virtually identical (*SI Appendix*, Fig. S1). Quantification of the signals revealed that levels of ^{79}Br and ^{81}Br, relative to ^{13}C, were greater in basement membranes than inside cells (*SI Appendix*, Figs. S1 and S2). Levels of ^{79}Br secondary ions were ∼2.6% greater than levels of ^{81}Br, consistent with the natural abundance of the two isotopes. There was little or no ^{127}I enrichment in basement membranes, relative to cells (*SI Appendix*, Fig. S2). We also observed bromine enrichment in the basement membranes lining capillary endothelial cells of the lung (*SI Appendix*, Fig. S3).

Bromine Localization in Normal and Diseased Human Glomeruli. Kidney biopsies (obtained for diagnostic purposes) are routinely processed for light and electron microscopy. We obtained archived resin-embedded kidney biopsy specimens and cut 500-nm sections for NanoSIMS analyses. We examined two biopsy specimens from allograft kidneys deemed free of histopathologic abnormalities (Figs. 4 and 5*A*). Mirroring our findings in mouse kidneys, NanoSIMS analyses of normal human kidneys revealed striking ^{79}Br and ^{81}Br enrichment in TBMs, BCBMs, and GBMs (Figs. 4 and 5*A*). We also observed intense bromine enrichment in the mesangial matrix within the glomerulus. We found lower, but detectable, bromine enrichment within the ECM between renal tubules. We did not observe ^{127}I enrichment in basement membranes of normal human kidney (*SI Appendix*, Fig. S4).

We performed NanoSIMS analyses (Fig. 5*B*) on kidney specimens from two patients with TBMN, which had been diagnosed based on both clinical findings and transmission electron microscopy measurements of GBM thickness (30). Many patients with TBMN have heterozygous mutations in the genes for α3 collagen IV (*COL4A3*) or α4 collagen IV (*COL4A4*) (30, 31), but genetic studies of TBMN are not routine and had not been performed in the two cases that we examined. ^{79}Br enrichment in the GBMs was lower in the two TBMN specimens than in the two normal specimens that we had examined (Fig. 5*C*); however, drawing firm conclusions about bromine enrichment in TBMN GBMs would require analyzing many more cases. In an Alport syndrome kidney specimen, we observed localized regions of bromine enrichment in the mesangial matrix, but bromine enrichment in the GBM was lower than in the two normal kidney specimens (*SI Appendix*, Fig. S5*A*). Again, however, we would not draw conclusions about bromine enrichment from a single case of Alport syndrome. We observed high levels of bromine enrichment in the mesangial matrix in a glomerulus from a patient with anti-GBM disease (*SI Appendix*, Fig. S5*B*).

Because the HOBr from eosinophil peroxidase is known to brominate proteins, we performed NanoSIMS analyses on a kidney specimen from a patient with biopsy-proven allergic-type acute interstitial nephritis with active injury and prominent eosinophilic infiltrates (*SI Appendix*, Fig. S6). We observed bromine enrichment in basement membranes; however, bromine enrichment in the interstitial ECM between tubules (where inflammatory infiltrates

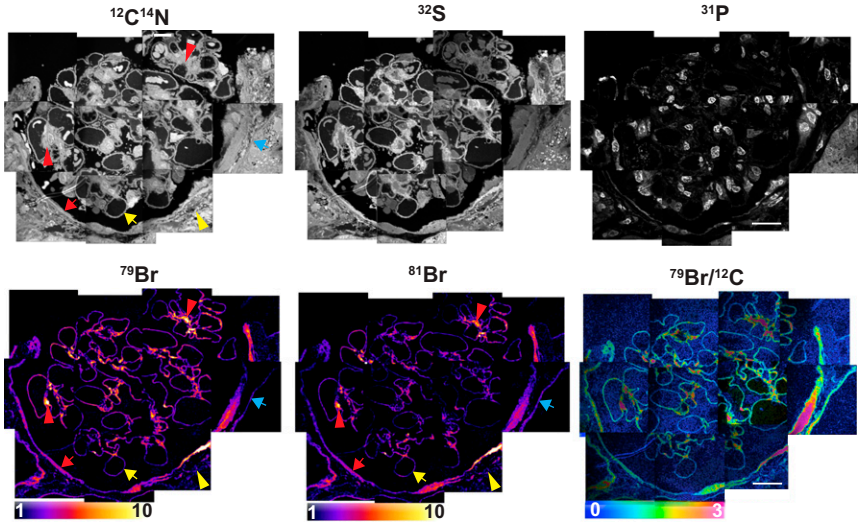

Fig. 4. Bromine enrichment in basement membranes of human kidney. A normal human kidney specimen was processed for NanoSIMS imaging. $^{12}C^{14}N$, ^{32}S, and ^{31}P NanoSIMS images were useful for visualizing morphology. ^{79}Br, ^{81}Br, and $^{79}Br/^{12}C$ images revealed bromine enrichment in the basement membrane of glomerular capillaries (yellow arrows), the basement membrane of renal tubules (blue arrows), and the basement membrane of Bowman's capsule (red arrows). There were several areas of intense bromine enrichment in the mesangial matrix of the glomerulus (red arrowheads). We also observed low amounts of bromine enrichment in the ECM outside of Bowman's capsule (yellow arrowheads). Quantification of the $^{79}Br/^{12}C$ ratios in glomerular capillaries is reported in Fig. 5. $^{79}Br/^{12}C$ ratios were multiplied by 10,000. (Scale bars: 20 μm.)

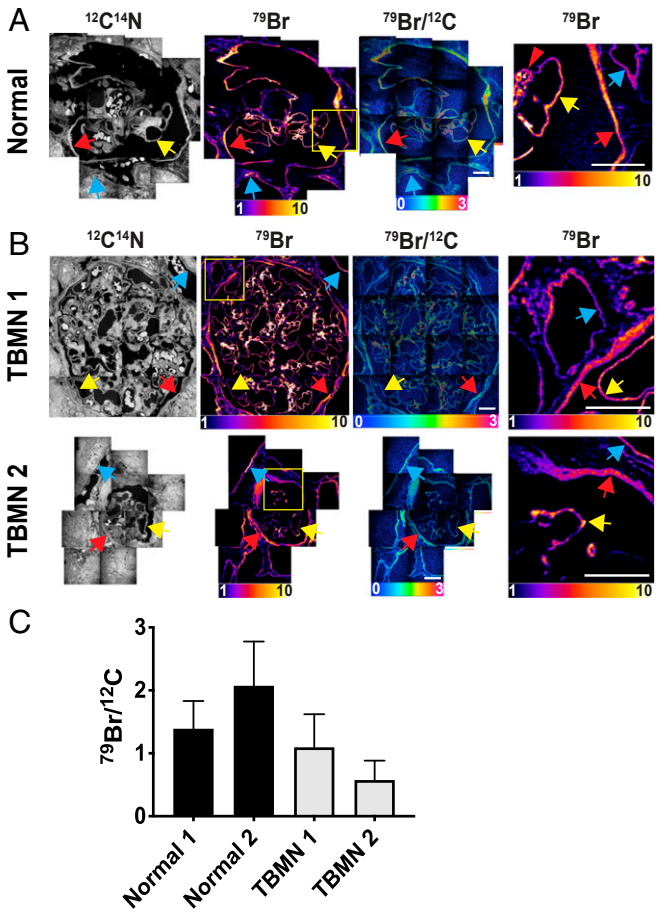

Fig. 5. Bromine enrichment of basement membranes from a normal human kidney (*A*) and two specimens from patients with TBMN (*B*). $^{12}C^{14}N$ NanoSIMS images were useful for visualizing morphology; ^{79}Br and $^{79}Br/^{12}C$ images were created to show bromine distribution and bromine enrichment in the GBM (yellow arrows), the renal tubule basement membrane (blue arrows), the basement membrane of Bowman's capsule (red arrows), and the mesangial matrix of the glomerulus (red arrowheads). The ^{79}Br images in the right-hand column are higher magnification images of the boxed regions of the images in the second column. $^{79}Br/^{12}C$ ratios are multiplied by 10,000. (Scale bars: 20 μm.) (*C*) Quantification of $^{79}Br/^{12}C$ ratios (mean ± SD) in glomerular capillary basement membranes for two normal human kidneys. NanoSIMS images for Normal 1 are shown in Fig. 4; images for Normal 2 are shown in *A*. Images for two TBMN specimens (TBMN 1, TBMN 2) are shown in *B*. The bar graph depicts the $^{79}Br/^{12}C$ ratio in 222 ROIs in glomerular capillaries of Normal 1; 57 ROIs for Normal 2; 442 ROIs for TBMN 1; and 28 ROIs for TBMN 2.

were present) was not greater than in the ECM of normal kidney specimens. This result was surprising, but it is conceivable that turnover of brominated proteins in the ECM is quite rapid or that the acute nature of the disease did not allow sufficient time for widespread bromination of the interstitial ECM. Drawing firm conclusions about protein bromination of the interstitial ECM in eosinophilic nephritis would require examining additional biopsy specimens, including specimens obtained at different time points during the course of the disease.

Because thickening of the GBM is a hallmark of diabetic nephropathy, we performed NanoSIMS imaging on kidney biopsy specimens from three patients with diabetic nephropathy (Fig. 6 and *SI Appendix*, Figs. S7, S8, and S9). As expected, the thickness of the GBMs, as judged by NanoSIMS images, was higher in the three diabetic nephropathy specimens (mean thickness of 967 nm, 29 capillaries measured) than in the two normal kidney specimens shown in Figs. 4 and 5*A* (mean thickness of 593 nm, 24 capillaries measured). Bromine enrichment in GBMs, normalized to carbon signals (^{12}C or ^{13}C), was ~37% higher in the diabetic nephropathy specimens (Fig. 6 and *SI Appendix*, Fig. S9) than in the normal kidney specimens (Figs. 4 and 5*A*). In the diabetic nephropathy specimens, we also observed bromine enrichment in the TBMs (Fig. 6). In the diabetic nephropathy specimen shown in Fig. 6 and *SI Appendix*, Fig. S9, bromine enrichment in GBMs was approximately twofold higher than in TBMs. Bromine enrichment was also observed in Kimmelstiel–Wilson nodules (Fig. 6). Bromine enrichment was also high in the basement membranes of atrophic renal tubules (Fig. 6 and *SI Appendix*, Fig. S8). In the specimen shown in Fig. 6*B*, the thick multilayered TBMs (typically found in atrophic tubules) was highly enriched in bromine.

Bromine Enrichment of Basement Membranes Is Peroxidasin-Dependent. We used NanoSIMS analyses to assess ^{79}Br enrichment and distribution in kidneys of wild-type and in peroxidasin knockout mice (*Pxdn*$^{-/-}$; homozygous for a *Pxdn* allele harboring a gene-trap insertion in intron 8) (*Materials and Methods*) (5). We observed no evidence of renal pathology in *Pxdn*$^{-/-}$ mice by BSE imaging (*SI Appendix*, Fig. S10). However, we observed markedly reduced amounts of ^{79}Br in GBMs from *Pxdn*$^{-/-}$ mice (Fig. 7*A* and *SI Appendix*, Fig. S11). Quantitative analyses of $^{79}Br^-$ secondary ions revealed that bromine enrichment in basement membranes was reduced by ~85% in *Pxdn*$^{-/-}$ mice (Fig. 7*B*); the extent of the reduction was similar in the TBMs, BCBMs, and GBMs (Fig. 7). The existence of some basement membrane bromination in the *Pxdn*$^{-/-}$ mice, combined with earlier observation of some sulfilimine bond formation in the same mice (32), raised our suspicions that the *Pxdn* gene-trap allele was leaky (with splicing around the gene-trap insertion). Indeed, quantitative RT-PCR studies of an amplicon spanning exons 8 and 9 sequences (across the insertional mutation) revealed evidence for the expression of normal *Pxdn* transcripts in gene-trap *Pxdn*$^{-/-}$ mice at a level of ~6.7% of those found in wild-type mice.

Because hypobromous acid is known to brominate tyrosine residues in proteins (33), we suspected that the reduced bromine enrichment in the basement membranes of *Pxdn*$^{-/-}$ mice would be mirrored by reduced amounts of bromotyrosine in basement membrane proteins. We identified, by liquid chromatography–tandem mass spectrometry (LC-MS/MS), a tyrosine bromination site in the carboxyl-terminal noncollagenous 1 (NC1) domain of the α2 collagen IV chain (COL4A2). Analysis of tryptic peptides revealed a bromine modification of COL4A2-Tyr^{1485} (Fig. 8 and *SI Appendix*, Table S1). The very same tyrosine was brominated in human kidney COL4A2 (*SI Appendix*, Table S1 and Fig. S12). The bromination of COL4A2-Tyr^{1485} was peroxidasin-dependent; bromination of that residue was reduced by ~93% in the NC1 domain of α2 collagen IV in kidneys of *Pxdn*$^{-/-}$ mice (Fig. 8*C*) (5). Bromination of Tyr^{1485} was undetectable in the NC1 domains isolated from the ECM of *Pxdn*-null mouse PFHR9 cells (32) (where peroxidasin expression was eliminated by CRISPR/CAS9 genome editing and sulfilimine bonds are not formed) (Fig. 9)

Discussion

The formation of sulfilimine cross-links between the NC1 domains of collagen IV trimers depends on the capacity of peroxidasin to use H_2O_2 and bromine substrates to produce HOBr, a potent oxidizing agent (1, 7, 13). Sulfilimine cross-links are crucial for the integrity of both collagen IV and the basement membrane (1, 3, 5). A longstanding puzzle, however, has been whether the HOBr released by peroxidasin acts selectively to promote collagen IV sulfilimine cross-links or whether it also results in oxidative damage to bystander molecules in the ECM (7, 22, 23): for example, by brominating tyrosine residues within proteins. After sulfilimine cross-links have been formed, bromide is presumably released into

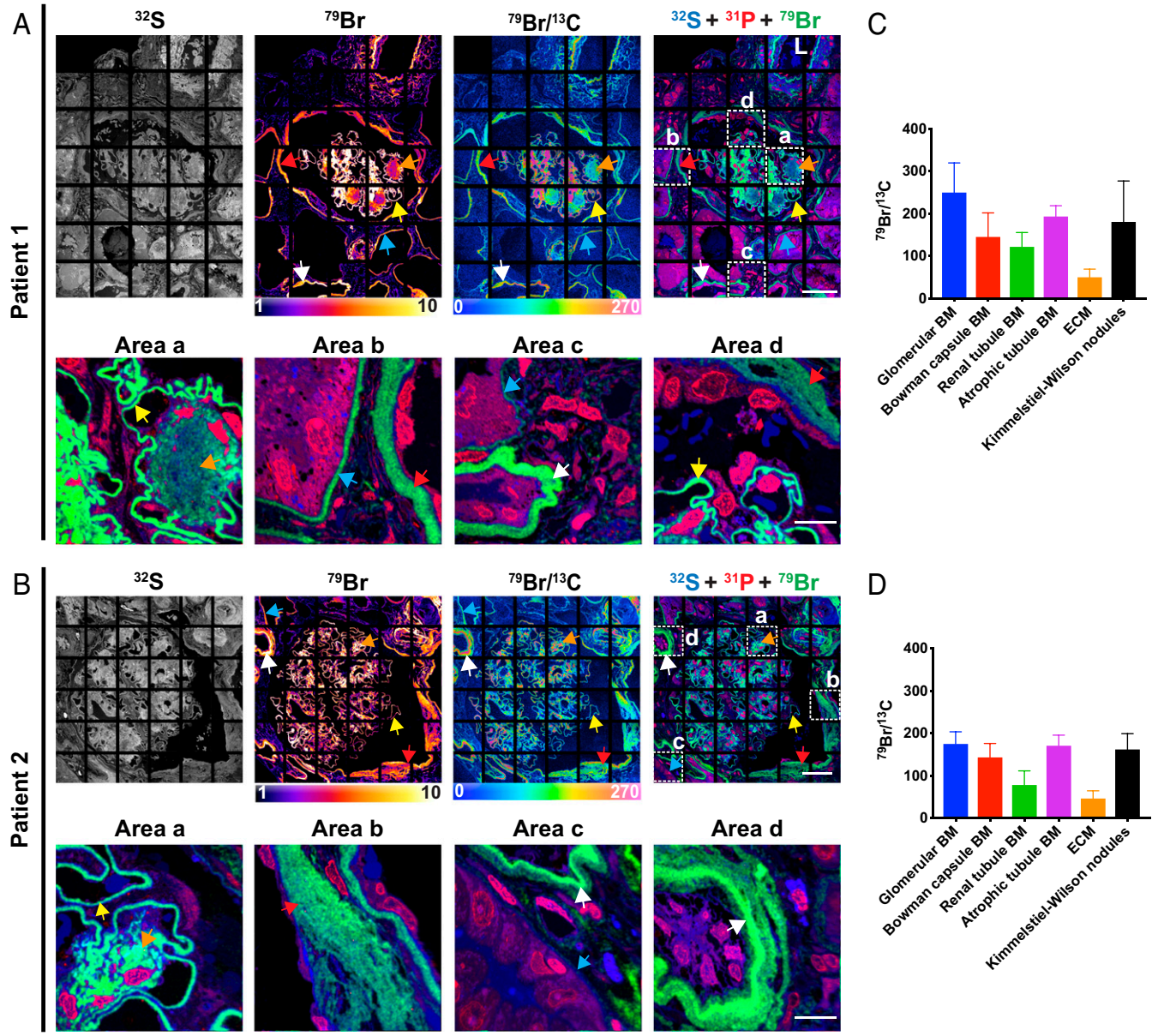

Fig. 6. NanoSIMS images reveal marked bromine enrichment in the GBMs of kidney biopsy specimens from two patients with diabetic nephropathy. (*A* and *B*) ^{32}S, ^{79}Br, $^{79}Br/^{13}C$, and composite ^{31}P (red), ^{32}S (blue), and ^{79}Br (green) NanoSIMS images of the kidney biopsies from two patients with diabetic nephropathy. Individual ^{13}C, $^{12}C^{14}N$, ^{31}P, ^{32}S, and ^{79}Br NanoSIMS images of the specimens in *A* and *B* are shown, respectively, in *SI Appendix*, Figs. S7 and S8. The *Lower* within *A* and *B* represent close-up images of boxed regions (area a, area b, area c, and area d) in the *Upper*. ^{79}Br, $^{79}Br/^{13}C$, and ^{31}P (red), ^{32}S (blue), and ^{79}Br (green) composite NanoSIMS images were generated to show bromine in the GBM (yellow arrows), the renal tubule basement membrane (BM) (blue arrows), the BM of Bowman's capsule (red arrows), the BM of atrophic renal tubules (white arrows), and Kimmelstiel–Wilson nodules (orange arrows). (*C*) Quantification of $^{79}Br/^{13}C$ ratio for ROIs (mean ± SD) in patient 1 specimen. Glomerular BM, $n = 144$ ROIs; Bowman capsule BM, $n = 67$ ROIs; renal tubule BM, $n = 191$ ROIs; atrophic renal tubule BM, $n = 17$ ROIs; ECM between renal tubules ($n = 105$ ROIs); Kimmelstiel–Wilson nodules, $n = 86$ ROIs. (*D*) Quantification of $^{79}Br/^{13}C$ ratio for ROIs (mean ± SD) in patient 2. Glomerular BM, $n = 196$ ROIs; Bowman capsule BM, $n = 105$ ROIs; renal tubule BM, $n = 12$ ROIs; atrophic renal tubule BM, $n = 54$ ROIs; ECM, $n = 33$ ROIs; and Kimmelstiel–Wilson nodules, $n = 191$ ROIs. $^{79}Br/^{13}C$ ratios were multiplied by 10,000. L, artery lumen. (Scale bars: *Upper*, 45 μm; *Lower*, 10 μm.)

the ECM and is available for recycling in the same cross-linking reaction. However, we hypothesized that we might find evidence for bromination of bystander ECM proteins by using NanoSIMS imaging (34–37) to visualize bromine distribution within tissues. In the current studies, we discovered, by NanoSIMS analyses, that the basement membranes in wild-type mouse kidneys and normal human kidneys are markedly enriched in bromine. We also observed bromine enrichment of basement membranes in kidney specimens from patients with TBMN, Alport syndrome, anti-GBM disease, and diabetes mellitus. We discovered that bromine enrichment of basement membranes is peroxidasin-dependent. In kidneys of *Pxdn*$^{-/-}$ mice, bromine enrichment of basement membranes was reduced by 85%. When we purified collagen IV NC1 domains from mouse and human kidney and examined tryptic peptides by mass spectrometry, we observed bromination of a tyrosine within the NC1 domain of COL4A2 (Tyr^{1485} in mouse and Tyr^{1490} in human). Bromination of Tyr^{1485} *Pxdn*$^{-/-}$ kidneys was 93% lower than in wild-type kidneys. In NC1 domains purified from a peroxidasin-null

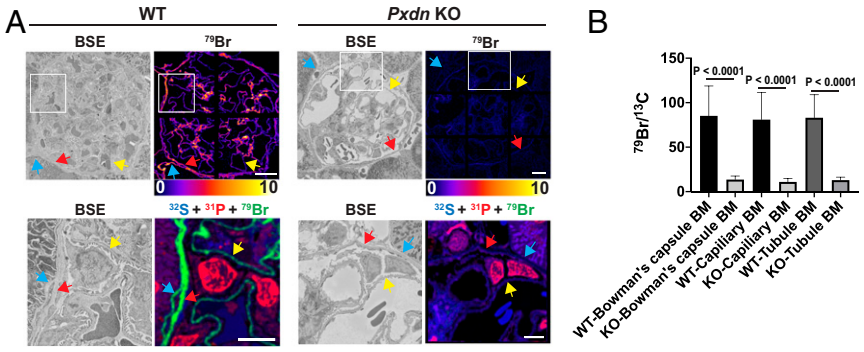

Fig. 7. Reduced amounts of bromine in BMs of kidneys from peroxidasin knockout (*Pxdn* KO) mice, as judged by NanoSIMS analyses. (*A*) Correlative BSE imaging and ^{79}Br NanoSIMS imaging of glomeruli in wild-type (WT) and *Pxdn* KO mice. (*Lower*) Higher magnification images of the boxed regions outlined in *Upper*. BSE images and composite ^{31}P (red), ^{32}S (blue), and ^{79}Br (green) NanoSIMS images of the same regions show bromine enrichment in the GBM (yellow arrows), the renal tubule BM (blue arrows), and the BM of Bowman's capsule (red arrows) of WT mice. Bromine enrichment was markedly reduced in the basement membranes of *Pxdn* KO mouse kidneys. (Scale bars, 10 μm.) (*B*) Quantification of bromine enrichment in basement membranes (mean ± SD) in kidneys of WT and *Pxdn* KO mice. ^{79}Br signals, normalized to ^{13}C signals, in wild-type Bowman's capsule basement membranes (WT-Bowman's capsule BM; n = 123 ROIs), *Pxdn* KO Bowman's capsule basement membranes (KO-Bowman's capsule BM; n = 88 ROIs), wild-type capillary basement membranes (WT-Capillary BM; n = 699 ROIs), *Pxdn* KO capillary basement membranes (KO-Capillary BM; n = 271 ROIs), wild-type kidney tubule basement membrane (WT-tubule BM; n = 102 ROIs), and *Pxdn* KO kidney tubule basement membrane (KO-tubule BM; n = 40 ROIs). ^{79}Br/^{13}C ratios were multiplied by 10,000.

cell line, bromination of Tyr^{1485} was undetectable. Thus, peroxidasin is responsible for the bromination of basement membranes (as judged by NanoSIMS analyses) and for bromination of a bystander tyrosine residue within the NC1 domain of α2 collagen IV (as judged by LC-MS/MS studies). Of note, bromination of tyrosine residues presumably represents only a subset of peroxidasin-mediated oxidation reactions. HOBr does not always generate bromine adducts; for example, it rapidly reacts with methionine and cysteine residues to generate methionine sulfoxide and cysteine sulfenic acid, respectively (38).

In the current studies, we examined *Pxdn*$^{-/-}$ mice (5) that had a gene-trap insertion in intron 8 (*Materials and Methods*). These "gene-trap" *Pxdn*$^{-/-}$ mice, like peroxidasin-deficient humans (8) and *Pxdn*$^{-/-}$ mice harboring a premature stop codon within the peroxidase domain (9), exhibited severe dysgenesis of the anterior segment of the eye. Despite the severity of the eye pathology in the gene-trap *Pxdn*$^{-/-}$ mice, we suspected (even before embarking on our studies) that the gene-trap allele might yield trace amounts of peroxidasin expression. This view is based upon the fact that collagen IV cross-links were easily detectable (about 30% of normal) in gene-trap *Pxdn*$^{-/-}$ mice (5) but were virtually absent in *Pxdn*$^{-/-}$ mice harboring a 2-base pair (bp) deletion near the beginning of the peroxidasin domain coding sequences (39). Our current studies heightened our suspicions that the gene-trap *Pxdn* allele might be "leaky." By NanoSIMS analyses, bromine enrichment in GBMs of the gene-trap *Pxdn*$^{-/-}$ mice was only reduced by ∼85% (rather than being eliminated), and, by mass spectrometry, bromination of Tyr^{1485} of COL4A2 from *Pxdn*$^{-/-}$ kidneys was reduced by 93% (rather than being eliminated). We suspect that bromine enrichment of the basement membrane would be completely eliminated in knockout mice harboring a bona fide *Pxdn*-null allele, given that bromination of Tyr^{1485} was undetectable in a peroxidasin-null cell line.

In *Drosophila*, peroxidasin is located in the basement membrane of muscle cells lining the gut (1, 3). In mammals, peroxidasin is assumed to be located in the ECM (23), but the localization of peroxidasin within the ECM has never been precisely defined, owing to an absence of useful antibody reagents. The fact that bromine enrichment in our NanoSIMS images of mice was largely restricted to basement membranes implies that peroxidasin activity is largely confined to the basement membrane. However, given that we observed small amounts of bromine in the interstitial spaces between renal tubules, it is possible that small amounts of peroxidasin are located outside of basement membranes. Of note, we observed peroxidasin-mediated bromine enrichment in basement membranes in Bowman's capsule (which contain α1α2α1 and α5α6α5 collagen IV networks) (40) and in the basement membranes between podocytes and endothelial cells of glomerular capillaries (which contain separate α1α2α1 and α3α4α5 collagen IV networks) (41, 42). Despite differences in sulfilimine bond formation in wild-type and *Pxdn*$^{-/-}$ mice (32) and the extent of bromination of kidney basement membranes, we observed no histologic differences by electron microscopy or NanoSIMS imaging. The only overt histopathologic abnormality resulting from peroxidasin deficiency is dysgenesis of the anterior chamber of the eye (9).

The fact that we were able to detect, by LC-MS/MS, peroxidasin-dependent bromination of Tyr^{1485} in the NC1 domain of mouse kidney α2 collagen IV indicates that the HOBr from peroxidasin modifies bystander tyrosine residues in proteins in addition to promoting sulfilimine cross-links. However, it is noteworthy that the bromination of the bystander tyrosine residues was not extensive. In our proteomic studies, only ∼1.5% of α2 chains of collagen IV in mouse kidney contained brominated Tyr^{1485}, and we never observed a doubly brominated tyrosine at that residue. Also, there are 58 tyrosine residues in the NC1 domains of α1α2α1 collagen IV hexamers, and only two of them (the Tyr^{1485} residues in the α2 chains) are brominated. Peroxidasin mutagenesis studies suggested that there are indirect interactions between peroxidasin Ig domains and collagen IV (6). We speculate that any such interactions are quite specific, such that the catalytic domain of peroxidasin—from which HOBr is released—is positioned in close proximity to Tyr^{1485} of the α2 (IV) chain and close to the methionine and hydroxylysine residues involved in sulfilimine cross-links. However, because Tyr^{1485} and the sulfilimine cross-links are located on opposite sides of α2 NC1 domains, peroxidasin positioning could be complicated and involve conformational changes.

Does bromination of Tyr^{1485} in the α2 collagen IV NC1 domain fully account for the ^{79}Br and ^{81}Br enrichment in mammalian basement membranes? Our data cannot answer this question in a definitive manner, simply because the NanoSIMS instrument merely records the release of ^{79}Br$^-$ and ^{81}Br$^-$ secondary ions. However, we are skeptical that the bromination of Tyr^{1485} is fully responsible for bromine enrichment of basement membranes. We suspect that the HOBr released by peroxidasin brominates other domains within collagen IV as well as other basement membrane proteins (perhaps including peroxidasin itself). If so, defining the location of additional bromotyrosine

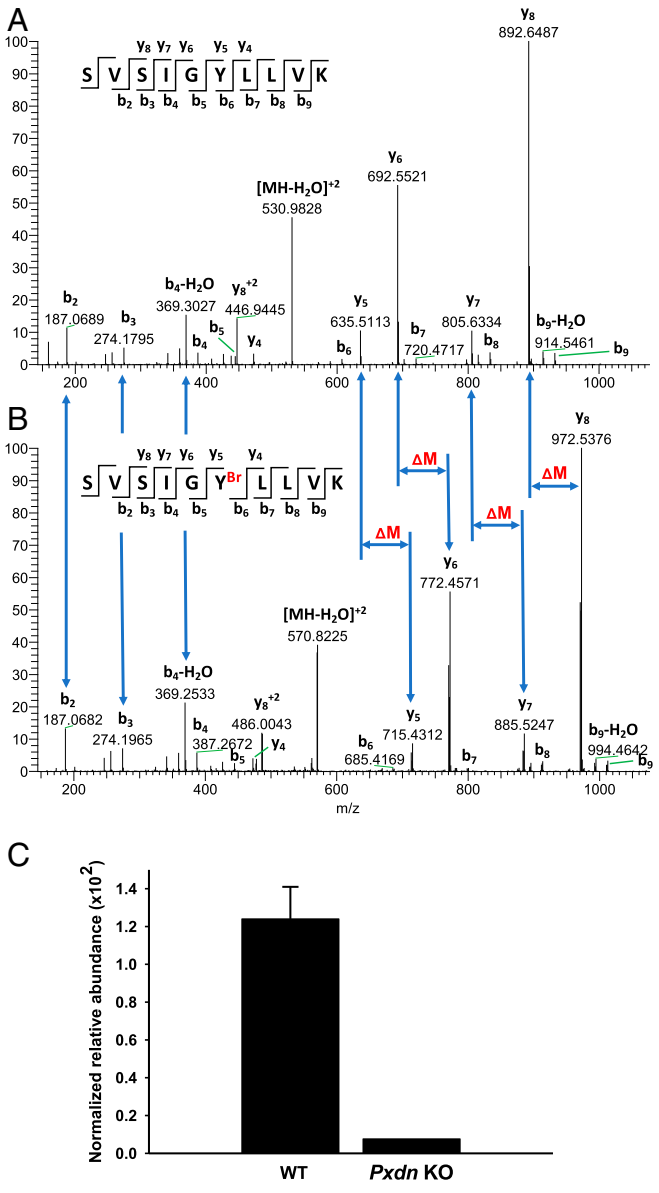

Fig. 8. Bromination site in the α2NC1 domain of collagen IV from mouse kidney and its dependence on peroxidasin expression. NC1 domains of collagen IV were isolated from WT and *Pxdn*$^{-/-}$ mice and analyzed by LC-MS/MS as described in *Materials and Methods*. (*A* and *B*) Evidence for bromination of Tyr^{1485} in a tryptic peptide of the α2NC1 domain of mouse collagen IV [α2(IV) NC1]. Shown are MS^2 spectra of unmodified (*A*) and brominated (*B*) peptide from the α2NC1 domain, including peak assignments. The mass shifts (ΔM) in y-ion series starting from y^5 and indicating the sequence position of brominated tyrosine residue are also shown. Masses of ^{79}Br and ^{81}Br isotopes calculated from the data in *A* and *B* were 78.9107 ± 0.0271 and 80.9086 ± 0.0143, respectively. The standard isotopic masses for ^{79}Br and ^{81}Br are 78.9183 and 80.9163, respectively. (*Insets*) The sequence of unmodified (*A*) and brominated (*B*) precursor peptide and the MS^2 fragmentation pattern producing specific y- and b-ions. The *y* axis in *A* and *B* is relative abundance. (*C*) Quantitation of the same brominated peptide in α2(IV)NC1 preparations from WT and *Pxdn*$^{-/-}$ mice. Normalized relative abundance represents modified peptide/(modified peptide + unmodified peptide). The WT data represent mean ± SD for three independent kidney NC1 preparations; the *Pxdn*$^{-/-}$ mouse data are from a preparation generated from the pooled kidneys of five *Pxdn*$^{-/-}$ mice.

residues could yield valuable insights into the positioning of peroxidasin's catalytic site within the basement membrane as well as the spatial relationships between different basement membrane proteins.

Our NanoSIMS analyses of diabetic nephropathy specimens were intriguing. The mechanism for GBM thickening in diabetes is not fully understood, but both increased synthesis and reduced turnover of basement membrane proteins have been proposed (43, 44). In our studies, we observed a high degree of bromine enrichment in the glomerular capillaries in diabetic nephropathy specimens. While this phenomenon could be due to increased expression of collagen IV and/or other basement membrane proteins, we are attracted to the idea that it is caused, at least in part, by reduced turnover of basement membrane proteins. Collagen IV as well as other basement membrane proteins (e.g., laminin, nidogen) are long-lived proteins (45), but a slower turnover rate would presumably increase tyrosine bromination by prolonging exposure to the HOBr produced by peroxidasin. It is possible, perhaps even likely, that the thickening of basement membranes in diabetes, along with peroxidasin-mediated bromination of basement membrane proteins, underlies higher bromotyrosine levels in the urine of patients with diabetes mellitus (46). In future studies, it should be possible to pursue that possibility in mouse models of diabetes, including in mice that are homozygous for *Pxdn*-null alleles.

Materials and Methods

Mouse Strains and Cells. Wild-type mice (strain C57BL/6) were purchased from The Jackson Laboratory. Peroxidasin-deficient mice (*Pxdn*$^{-/-}$; strain C57BL/6) were generated by Bhave et al. (5). These *Pxdn*$^{-/-}$ mice were generated with a targeting vector from the Knockout Mouse Project (KOMP) Repository (Project ID CSD 80013; https://www.komp.org/) and contained a gene-trap cassette in intron 8. Additional details regarding *Pxdn* mouse models and experimental methods for quantifying *Pxdn* transcripts in mouse tissues are described in *SI Appendix, Materials and Methods*. *Pxdn*-null PFHR9 cells were generated and characterized by Colon and Bhave (32).

Sample Preparation of Mouse Tissues for Electron Microscopy and NanoSIMS Analyses. Mouse tissues were fixed at 4 °C overnight in a solution containing 4% paraformaldehyde, 2.5% glutaraldehyde, and 2.1% sucrose in 0.1 M sodium cacodylate. On the following day, tissues were rinsed five times for 3 min with 0.1 M sodium cacodylate and then incubated in a 0.1-M sodium cacodylate solution containing 2% osmium tetroxide and 1.5% potassium ferricyanide for 1 h at 4 °C. The samples were then rinsed five times for 3 min with distilled water before being incubated with 1% thiocarbohydrazide for 20 min at room temperature. Next, samples were rinsed five times for 3 min with distilled water and then incubated with 2% osmium tetroxide for 30 min at room temperature. The samples were then rinsed five times for 3 min each with distilled water and incubated with 2% uranyl acetate at 4 °C overnight. On the following day, the samples were rinsed with distilled water and then dehydrated by incubating the samples in progressively increasing amounts of ethanol (30, 50, 70, 85, 95, and 100%) for 10 min each followed by two additional 10-min incubations with 100% ethanol. Next, the samples were infiltrated with Embed812 resin (Electron Microscopy Sciences) by incubating the samples in 33% resin (diluted in anhydrous acetone) for 2 h, 66% resin overnight, and 100% resin for 4 h. Samples were then embedded in fresh resin with polypropylene molds (Electron Microscopy Sciences) and polymerized in a vacuum oven at 65 °C for 48 h.

Preparation of Human Kidney Biopsies for NanoSIMS Analyses. Archived resin blocks from renal biopsies were obtained from the Translational Pathology Core Laboratory (TPCL), a College of American Pathologists/Clinical Laboratory Improvement Acts (CAP/CLIA)-certified research facility that was established as an institutional resource by the David Geffen School of Medicine at the University of California, Los Angeles (UCLA). The TPCL is administered by UCLA's Department of Pathology and Laboratory Medicine. Permission to utilize archived kidney biopsy material for this collaborative study was requested by J.E.Z., a UCLA renal pathologist and coauthor on this paper. J.E.Z.'s request was reviewed and approved by UCLA's Human Use Institutional Review Board (IRB) (no. 19-002243). No other coauthor was aware of patient information. Kidney biopsies from patients with biopsy-proven TBMN, Alport syndrome, anti-GBM disease, allergic-type acute interstitial nephritis, and diabetic nephropathy were identified; the biopsy diagnoses were confirmed based on a review of original biopsy material and patient information by J.E.Z. Kidney donor transplant biopsy specimens with no significant pathologic changes were used for the "normal" controls.

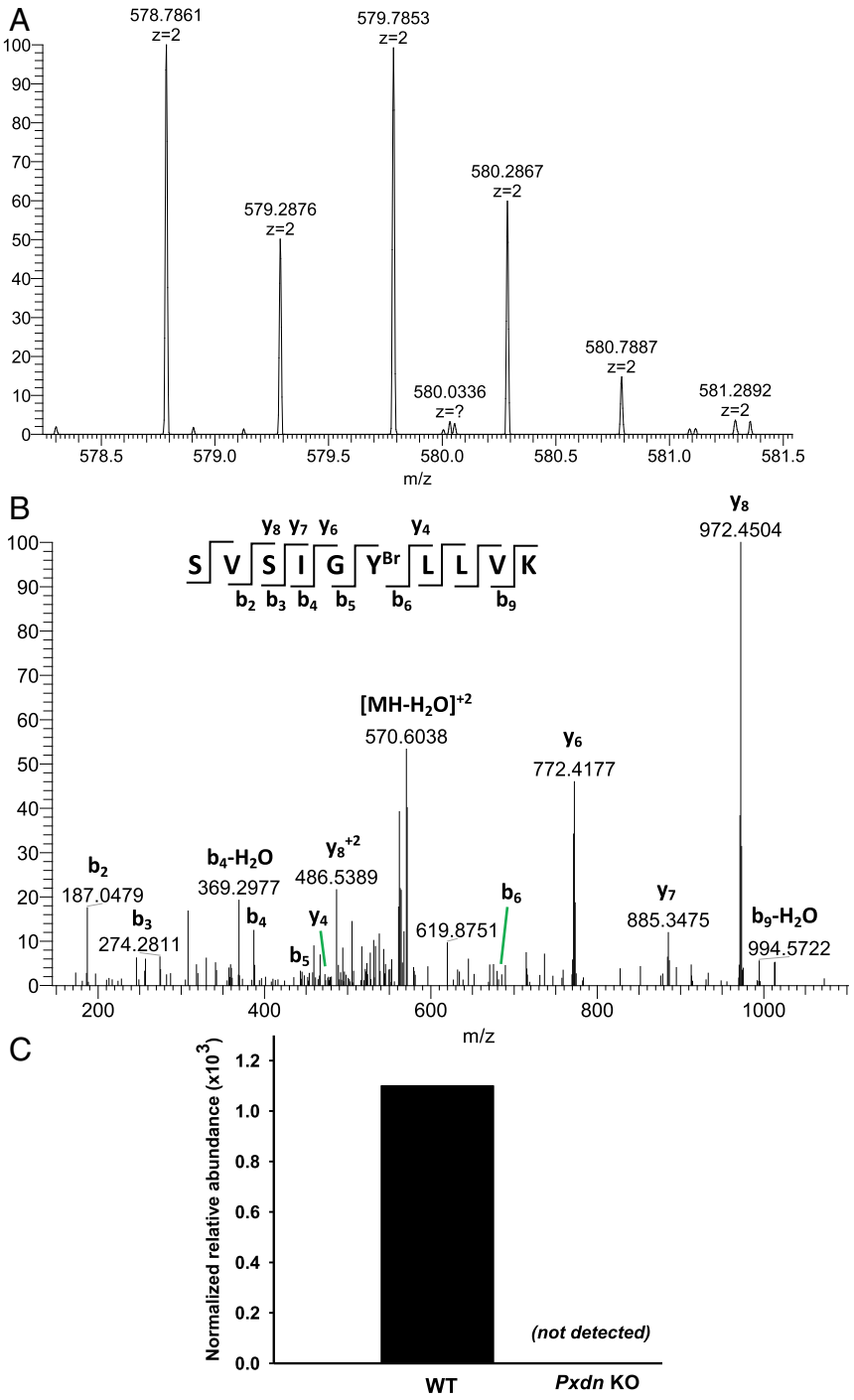

Fig. 9. Bromination site in the α2NC1 domain of collagen IV from the ECM deposited by cultured PFHR9 cells and its dependence on peroxidasin expression. NC1 domains of collagen IV were isolated from ECM deposited by WT and *Pxdn*-deficient PFHR9 cells (*Pxdn* KO) and analyzed by LC-MS/MS as described in *Materials and Methods*. (*A*) Isotopic envelope of brominated precursor peptide, revealing a characteristic bromine pattern deriving from the presence of ^{79}Br and ^{81}Br isotopes (mass accuracy is 3.3 parts per million [ppm]). (*B*) The MS^2 spectra of the brominated peptide, including peak assignments. (*Inset*) The sequence of brominated precursor peptide and the MS^2 fragmentation pattern producing specific y- and b-ions. (*C*) Quantification of tyrosine bromination in the tryptic peptide from α2(IV)NC1 preparations derived from the matrix of WT PFHR9 cells and *Pxdn*-deficient PFHR9 cells. Normalized relative abundance represents modified peptide/(modified peptide + unmodified peptide). The WT and *Pxdn* KO data represent single preparations, each deriving from the ECM collected from four 150-mm cell culture dishes.

At the time of original biopsy, fresh tissue was placed in a 0.1-M sodium cacodylate buffer, pH 7.4, containing 2.5% glutaraldehyde and 2.0% paraformaldehyde for a minimum of 2 h at room temperature and then washed with 0.1 M sodium cacodylate. Tissue was fixed in 1% osmium tetroxide in 0.1 M sodium cacodylate for 1.5 to 2 h and again washed in the 0.1 M sodium cacodylate buffer. Next, the tissue was dehydrated through an acetone gradient and infiltrated with epon resin. Epon-embedded tissue was warmed in a 65 to 85 °C oven for 40 min and embedded into predried molds. Polymerization was allowed to occur at 65 to 85 °C overnight.

Scanning Electron Microscopy. Five hundred-nanometer sections of resin-embedded mouse tissues were prepared with a Leica UC6 ultramicrotome and mounted onto silicon wafers. BSE images were obtained with an FEI Verios scanning electron microscope (Thermo Fisher) with a 1-kV beam with the current at 200 pA.

NanoSIMS Analyses. Five hundred-nanometer sections of resin-embedded tissues were cut with a Leica UC6 ultramicrotome and mounted onto silicon wafers. Sections were then coated with 5 nm of gold and analyzed with either NanoSIMS 50 or NanoSIMS 50L instruments (CAMECA). Samples were bombarded with a focused 16-KeV $^{133}Cs^+$ beam, and both secondary electrons (SEs) and secondary ions ($^{12}C^-$ or $^{13}C^-$,$^{12}C^{14}N^-$ or $^{13}C^{14}N^-$, $^{31}P^-$, $^{32}S^-$, $^{79}Br^-$ and/or $^{81}Br^-$, $^{127}I^-$) were collected. In some experiments, correlative BSE imaging and NanoSIMS analyses were performed on the same tissue section. NanoSIMS instrument settings are described in *SI Appendix, Materials and Methods*.

Images were processed and prepared with the OpenMIMS plugin in ImageJ. ^{79}Br, ^{81}Br, and ^{127}I images were processed with a Gaussian Blur filter in ImageJ with a radius of 1 to reduce noise. For image quantification, regions of interest (ROIs) were drawn manually based on the morphological features in NanoSIMS and BSE images. ^{79}Br, ^{81}Br, and ^{127}I in ROIs, normalized to ^{13}C or ^{12}C, were extracted using the OpenMIMS plugin and processed by GraphPad Prism 7.0. Comparisons between bromine enrichment measurements normalized to ^{12}C or ^{13}C (natural abundance, 1.1%) were calculated by $^{79}Br/^{12}C = (^{79}Br/^{13}C)/89.9$.

Isolation of Collagen IV NC1 Domains from Mouse Kidneys and the ECM Deposited by Cultured Cells. Collagen IV NC1 domains were isolated from kidney tissue as described (47) with minor modifications. Kidneys were homogenized in 50 mM Tris·HCl buffer, pH 7.4, supplemented with 150 mM NaCl, 20 mM ethylenediaminetetraacetic acid, 25 mM ε-aminocaproic acid, 5 mM benzamidine, 5 mM *N*-ethylmaleimide, 1 mM phenylmethylsulfonylfluoride (PMSF), and 1 μg/mL each of three protease inhibitors (leupeptin, pepstatin A, aprotinin), followed by stirring for 1 h at 4 °C and centrifugation at 8,000 × *g* for 15 min. This procedure was repeated three times with fresh buffer, and the pellets were resuspended in ice-cold water with 0.05% sodium azide and 1 mM PMSF. The suspension was stirred for 1 h at 4 °C, followed by centrifugation at 8,000 × *g* for 15 min. The pellets were then resuspended in 1 M NaCl and incubated with 200 Kunitz U/mL of DNase, followed by stirring for 2 h at room temperature and centrifugation at 8,000 × *g* for 15 min. The pellet was resuspended in ice-cold water, gradually adding sodium deoxycholate to a final concentration of 1% and stirring at room temperature for 2 h. Pellets were digested with collagenase (20 U/mL) for 24 h at 37 °C with stirring (48). The digested material was dialyzed against 50 mM Tris·HCl, pH 7.5, and then loaded onto a diethylaminoethyl (DEAE) Sepharose column. A pass-through fraction from the DEAE column was collected and purified with a Superdex 200 10/300 GL gel-filtration column (GE Healthcare) (49).

Isolation of collagen IV NC1 domains from the ECM deposited by cultured PFHR9 cells was performed as described (50). Briefly, confluent parental PFHR9 cells or *Pxdn*-deficient PFHR9 cells (32) were maintained in Dulbecco's modified Eagle's medium for 7 d in the presence of 50 μg/mL ascorbic acid with daily medium changes. Cells were then washed in phosphate-buffered saline and scraped into 1% (wt/vol) sodium deoxycholate lysis buffer. The lysates were sonicated to shear genomic DNA, and the insoluble material was collected by centrifugation at 20,000 × *g*, washed twice in 1 M NaCl and 10 mM Tris·HCl, and then resuspended in 50 mM Tris·HCl, pH 7.4. The matrix material was digested with bacterial collagenase (20 U/mL; Worthington Biochemical Corporation) in a buffer containing 5 mM $CaCl_2$, 5 mM benzamidine, 25 mM ε-aminocaproic acid, and 0.4 mM PMSF. Digests were cleared by centrifugation at 15,000 × *g* for 5 min, dialyzed against 50 mM Tris·HCl (pH 7.5), and purified on a DEAE Sepharose column, followed by a Superdex 200 10/300 GL gel-filtration column (49). Purified NC1 collagen IV hexamers were concentrated with Amicon Ultra Centrifugal Filter Units (10,000 molecular weight cutoff).

LC-MS/MS Analyses of Bromination Sites. Bromination sites in the collagen IV NC1 domains from kidneys or from the ECM deposited by cultured cells were analyzed by LC-MS/MS in the Proteomics Core of the Vanderbilt Mass Spectrometry Research Center (51). Sample preparations and MS^2 spectra generation and analyses are described in *SI Appendix, Materials and Methods*.

Institutional Approvals. Animal protocols were approved by institutional Animal Research Committees (UCLA, Vanderbilt). Mice were fed a chow diet and housed in AAALAC (Association for Assessment and Accreditation of Laboratory Animal Care International)-approved facilities with a 12-h light–dark cycle. Archived samples of human kidney biopsies were obtained with approval from UCLA's Institutional Review Board (IRB no. 19-002243).

Statistics. Statistical analyses were performed with GraphPad Prism 7.0 software. Differences were assessed using a Student's *t* test with Welch's correction.

Data Availability. Data are included in the figures of this paper.

ACKNOWLEDGMENTS. This work was supported by National Heart, Lung, and Blood Institute Grants HL090553, HL087228, and HL125335 (to S.G.Y.); an Australian Research Council Discovery Early Career Researcher Award (to H.J.); NIH Grant R01 DK116964 and a Burroughs Welcome Fund Career Award for Medical Scientists (13030995) (to G.B.); and NIH Grants R01 DK065138 (to B.G.H. and P.A.V.) and R24 DK103067 (to B.G.H., in part). We thank Dr. Vadim Pedchenko (Division of Nephrology, Vanderbilt University Medical Center) for providing samples of NC1 domains from human renal cortical shavings, Dr. Kristie Lindsey Rose (Mass Spectrometry Research Center, Vanderbilt University) for suggestions on experimental design and data analysis, and Dr. Maximiliano Gutierrez (The Francis Crick Institute) for helpful discussions. We thank the Centre for Microscopy, Characterisation & Analysis at the University of Western Australia, which is funded by the University and both the State and Commonwealth Governments.

1. A. S. McCall *et al*., Bromine is an essential trace element for assembly of collagen IV scaffolds in tissue development and architecture. *Cell* **157**, 1380–1392 (2014).
2. A. L. Fidler *et al*., Collagen IV and basement membrane at the evolutionary dawn of metazoan tissues. *eLife* **6**, e24176 (2017).
3. G. Bhave *et al*., Peroxidasin forms sulfilimine chemical bonds using hypohalous acids in tissue genesis. *Nat. Chem. Biol.* **8**, 784–790 (2012).
4. A. L. Fidler *et al*.; Aspirnauts, A unique covalent bond in basement membrane is a primordial innovation for tissue evolution. *Proc. Natl. Acad. Sci. U.S.A.* **111**, 331–336 (2014).
5. G. Bhave, S. Colon, N. Ferrell, The sulfilimine cross-link of collagen IV contributes to kidney tubular basement membrane stiffness. *Am. J. Physiol. Renal Physiol.* **313**, F596–F602 (2017).
6. I. A. Ero-Tolliver, B. G. Hudson, G. Bhave, The ancient immunoglobulin domains of peroxidasin are required to form sulfilimine cross-links in collagen IV. *J. Biol. Chem.* **290**, 21741–21748 (2015).
7. S. Colon, P. Page-McCaw, G. Bhave, Role of hypohalous acids in basement membrane homeostasis. *Antioxid. Redox Signal.* **27**, 839–854 (2017).
8. A. Choi *et al*., Novel mutations in PXDN cause microphthalmia and anterior segment dysgenesis. *Eur. J. Hum. Genet.* **23**, 337–341 (2015).
9. X. Yan *et al*., Peroxidasin is essential for eye development in the mouse. *Hum. Mol. Genet.* **23**, 5597–5614 (2014).
10. K. Khan *et al*., Homozygous mutations in PXDN cause congenital cataract, corneal opacity, and developmental glaucoma. *Am. J. Hum. Genet.* **89**, 464–473 (2011).
11. S. J. Klebanoff, A. J. Kettle, H. Rosen, C. C. Winterbourn, W. M. Nauseef, Myeloperoxidase: A front-line defender against phagocytosed microorganisms. *J. Leukoc. Biol.* **93**, 185–198 (2013).
12. N. E. Hansen, H. Karle, V. Andersen, J. Malmquist, G. E. Hoff, Neutrophilic granulocytes in acute bacterial infection. Sequential studies on lysozyme, myeloperoxidase and lactoferrin. *Clin. Exp. Immunol.* **26**, 463–468 (1976).
13. S. J. Weiss, S. T. Test, C. M. Eckmann, D. Roos, S. Regiani, Brominating oxidants generated by human eosinophils. *Science* **234**, 200–203 (1986).
14. N. M. Nogueira, S. J. Klebanoff, Z. A. Cohn, T. cruzi: Sensitization to macrophage killing by eosinophil peroxidase. *J. Immunol.* **128**, 1705–1708 (1982).
15. J. Buys, R. Wever, R. van Stigt, E. J. Ruitenberg, The killing of newborn larvae of Trichinella spiralis by eosinophil peroxidase in vitro. *Eur. J. Immunol.* **11**, 843–845 (1981).
16. S. Specht *et al*., Lack of eosinophil peroxidase or major basic protein impairs defense against murine filarial infection. *Infect. Immun.* **74**, 5236–5243 (2006).
17. S. Colon *et al*., Peroxidasin and eosinophil peroxidase, but not myeloperoxidase, contribute to renal fibrosis in the murine unilateral ureteral obstruction model. *Am. J. Physiol. Renal Physiol.* **316**, F360–F371 (2019).
18. R. E. Aldridge *et al*., Eosinophil peroxidase produces hypobromous acid in the airways of stable asthmatics. *Free Radic. Biol. Med.* **33**, 847–856 (2002).
19. W. Wu *et al*., Eosinophils generate brominating oxidants in allergen-induced asthma. *J. Clin. Invest.* **105**, 1455–1463 (2000).
20. I. Mohiuddin *et al*., Nitrotyrosine and chlorotyrosine: Clinical significance and biological functions in the vascular system. *J. Surg. Res.* **133**, 143–149 (2006).
21. S. L. Hazen, J. R. Crowley, D. M. Mueller, J. W. Heinecke, Mass spectrometric quantification of 3-chlorotyrosine in human tissues with attomole sensitivity: A sensitive and specific marker for myeloperoxidase-catalyzed chlorination at sites of inflammation. *Free Radic. Biol. Med.* **23**, 909–916 (1997).
22. B. Bathish, R. Turner, M. Paumann-Page, A. J. Kettle, C. C. Winterbourn, Characterisation of peroxidasin activity in isolated extracellular matrix and direct detection of hypobromous acid formation. *Arch. Biochem. Biophys.* **646**, 120–127 (2018).

23. Z. Péterfi *et al*., Peroxidasin is secreted and incorporated into the extracellular matrix of myofibroblasts and fibrotic kidney. *Am. J. Pathol.* **175**, 725–735 (2009).
24. J. Kruegel, D. Rubel, O. Gross, Alport syndrome–Insights from basic and clinical research. *Nat. Rev. Nephrol.* **9**, 170–178 (2013).
25. S. D. Funk, M. H. Lin, J. H. Miner, Alport syndrome and Pierson syndrome: Diseases of the glomerular basement membrane. *Matrix Biol.* **71–72**, 250–261 (2018).
26. B. G. Hudson, K. Tryggvason, M. Sundaramoorthy, E. G. Neilson, Alport's syndrome, Goodpasture's syndrome, and type IV collagen. *N. Engl. J. Med.* **348**, 2543–2556 (2003).
27. K. Rana *et al*., The genetics of thin basement membrane nephropathy. *Semin. Nephrol.* **25**, 163–170 (2005).
28. V. Pedchenko *et al*., Molecular architecture of the Goodpasture autoantigen in anti-GBM nephritis. *N. Engl. J. Med.* **363**, 343–354 (2010).
29. N. Papadopoulou-Marketou, G. P. Chrousos, C. Kanaka-Gantenbein, Diabetic nephropathy in type 1 diabetes: A review of early natural history, pathogenesis, and diagnosis. *Diabetes Metab. Res. Rev.* **33**, e2841 (2017).
30. M. Haas, Alport syndrome and thin glomerular basement membrane nephropathy: A practical approach to diagnosis. *Arch. Pathol. Lab. Med.* **133**, 224–232 (2009).
31. P. Plevová, J. Gut, J. Janda, Familial hematuria: A review. *Medicina (Kaunas)* **53**, 1–10 (2017).
32. S. Colon, G. Bhave, Proprotein convertase processing enhances peroxidasin activity to reinforce collagen IV. *J. Biol. Chem.* **291**, 24009–24016 (2016).
33. W. Wu, Y. Chen, A. d'Avignon, S. L. Hazen, 3-Bromotyrosine and 3,5-dibromotyrosine are major products of protein oxidation by eosinophil peroxidase: Potential markers for eosinophil-dependent tissue injury in vivo. *Biochemistry* **38**, 3538–3548 (1999).
34. H. Jiang *et al*., High-resolution imaging of dietary lipids in cells and tissues by NanoSIMS analysis. *J. Lipid Res.* **55**, 2156–2166 (2014).
35. H. Jiang *et al*., Stable isotope imaging of biological samples with high resolution secondary ion mass spectrometry and complementary techniques. *Methods* **68**, 317–324 (2014).
36. C. He *et al*., NanoSIMS analysis of intravascular lipolysis and lipid movement across capillaries and into cardiomyocytes. *Cell Metab.* **27**, 1055–1066.e3 (2018).
37. C. He *et al*., High-resolution imaging and quantification of plasma membrane cholesterol by NanoSIMS. *Proc. Natl. Acad. Sci. U.S.A.* **114**, 2000–2005 (2017).
38. D. I. Pattison, M. J. Davies, Kinetic analysis of the reactions of hypobromous acid with protein components: Implications for cellular damage and use of 3-bromotyrosine as a marker of oxidative stress. *Biochemistry* **43**, 4799–4809 (2004).
39. G. Sirokmány *et al*., Peroxidasin-mediated crosslinking of collagen IV is independent of NADPH oxidases. *Redox Biol.* **16**, 314–321 (2018).
40. Y. Ninomiya *et al*., Differential expression of two basement membrane collagen genes, COL4A6 and COL4A5, demonstrated by immunofluorescence staining using peptide-specific monoclonal antibodies. *J. Cell Biol.* **130**, 1219–1229 (1995).
41. L. Heidet, Y. Cai, L. Guicharnaud, C. Antignac, M. C. Gubler, Glomerular expression of type IV collagen chains in normal and X-linked Alport syndrome kidneys. *Am. J. Pathol.* **156**, 1901–1910 (2000).
42. H. Suleiman *et al*., Nanoscale protein architecture of the kidney glomerular basement membrane. *eLife* **2**, e01149 (2013).
43. W. Kriz *et al*., Accumulation of worn-out GBM material substantially contributes to mesangial matrix expansion in diabetic nephropathy. *Am. J. Physiol. Renal Physiol.* **312**, F1101–F1111 (2017).
44. F. N. Ziyadeh, Renal tubular basement membrane and collagen type IV in diabetes mellitus. *Kidney Int.* **43**, 114–120 (1993).
45. P. Liu, X. Xie, J. Jin, Isotopic nitrogen-15 labeling of mice identified long-lived proteins of the renal basement membranes. *Sci. Rep.* **10**, 5317 (2020).
46. Y. Kato *et al*., Quantification of modified tyrosines in healthy and diabetic human urine using liquid chromatography/tandem mass spectrometry. *J. Clin. Biochem. Nutr.* **44**, 67–78 (2009).
47. J. W. Fox, R. J. Butkowski, B. G. Hudson, Detergent-prepared glomerular basement membrane is composed of a heterogeneous group of polypeptides. *J. Biol. Chem.* **256**, 9313–9315 (1981).
48. J. Wieslander, M. Kataja, B. G. Hudson, Characterization of the human Goodpasture antigen. *Clin. Exp. Immunol.* **69**, 332–340 (1987).
49. T. Z. Kahsai *et al*., Seminiferous tubule basement membrane. Composition and organization of type IV collagen chains, and the linkage of alpha3(IV) and alpha5(IV) chains. *J. Biol. Chem.* **272**, 17023–17032 (1997).
50. S. P. Boudko, N. Danylevych, B. G. Hudson, V. K. Pedchenko, Basement membrane collagen IV: Isolation of functional domains. *Methods Cell Biol.* **143**, 171–185 (2018).
51. H. Madu *et al*., Pyridoxamine protects proteins from damage by hypohalous acids in vitro and in vivo. *Free Radic. Biol. Med.* **89**, 83–90 (2015).